Molecular Simulation of Dioleoylphosphatidylcholine Lipid Bilayers at Differing Levels of Hydration

R. Jay Mashl,* H. Larry Scott,† Shankar Subramaniam,‡ and Eric Jakobsson*

*Center for Biophysics and Computational Biology, National Center for Supercomputing Applications, Beckman Institute, University of Illinois, Urbana, Illinois 61801, †Department of Physics, Oklahoma State University, Stillwater, Oklahoma 74078, and ‡Bioengineering Department and San Diego Supercomputer Center, University of California at San Diego, San Diego, California 92037 USA

ABSTRACT The structure and dynamics of the lipid and water components of dioleoylphosphatidylcholine bilayers at various levels of hydration were studied using molecular dynamics (MD) simulations. Equilibration of these systems proceeded by use of a hybrid MD and configurational-bias Monte Carlo technique using one atmosphere of pressure normal to the membrane and a set point for the lateral area derived from experimental Bragg spacings, combined with experimentally derived specific volumes for each of the system components. Membrane surface tensions were observed to be of the order of tens of dyn/cm. The transbilayer molecular fragment peak positions at low hydration were found to agree with experimental neutron and x-ray scattering profiles and previously published simulations. For hydration levels of 5.4, 11.4, and 16 waters/lipid, molecular fragment distributions and order parameters for the headgroup, lipid chains, and water were quantified. Spin-lattice relaxation rates and lateral self-diffusion coefficients of water agreed well with results from experimental nuclear magnetic resonance studies. Relaxation rates of the choline segments and chemical shift anisotropies for the phosphate and carbonyls were computed. Headgroup orientation, as measured by the P-N vector, showed enhanced aligment with the membrane surface at low hydration. The sign of the membrane dipole potential reversed at low hydration, with the membrane interior negative relative to the interlamellar region. Calculation of the number of water molecules in the headgroup hydration shell, as a function of hydration level, supports the hypothesis that the break point in the curve of Bragg spacing versus hydration level near 12 waters/lipid, observed experimentally by Hristova and White (1998. *Biophys. J.* 74:2419–2433), marks the completion of the first hydration shell.

INTRODUCTION

Biological membranes are inherently multicomponent systems that include saturated and unsaturated lipid molecules that are in contact with water. Studies of pure lipid bilayers, however, remain essential to gain insight into the structure and dynamics of membranes. For example, the units of unsaturation in the acyl chains favor bilayers to be in a fluid state at biologically relevant temperatures. Experimental approaches have produced an abundance of structural data on lipid bilayers using x-ray scattering (Wiener and White, 1992a; Tristram-Nagle et al., 1993, 1998; Hristova and White, 1998; McIntosh, 1990), neutron scattering (Wiener and White, 1992a), NMR (Seelig, 1977; Brown et al., 1983; Bloom et al., 1991; Ulrich and Watts, 1994; Volke et al., 1994; Zhou et al., 1999), and infrared spectroscopy (Wong and Mantsch, 1988; Mendelsohn and Senak, 1993). Computer simulation models can assist in the understanding of experiments, in part by providing a level of detail that is experimentally unavailable or difficult to obtain (Pastor, 1994; Merz and Roux, 1996; Tieleman et al., 1997; Jakobsson, 1997; Feller et al., 1999).

Received for publication 13 January 2000 and in final form 13 September 2001.

Dr. Scott's present address is Illinois Institute of Technology, Chicago, IL 60616.

Address reprint requests to Dr. R. Jay Mashl, University of Illinois, NCSA, Beckman Institute, 405 N. Mathews Ave., Urbana, IL 61801. Tel.: 217-244-5818; Fax: 217-244-2909; E-mail: mashl@ncsa.uiuc.edu.

0006-3495/01/12/3005/11 $2.00

Although there have been numerous computer simulation studies of lipid bilayers with saturated chains (Venable et al., 1993; Stouch, 1993; Egberts et al., 1994; Damodaran and Merz, 1994; Feller et al., 1994; Huang et al., 1994; Chiu et al., 1995, 1999a; Tu et al., 1995; Tieleman and Berendsen, 1996; Berger et al., 1997; Husslein et al., 1998; Lindahl and Edholm, 2000), there have been relatively few simulation studies of lipid bilayers of unsaturated lipids, in particular, dioleoylphosphatidylcholine (DOPC) bilayers. Simulations of DOPC bilayers have previously focused on either low hydration (Huang et al., 1994; Feller et al., 1997; Armen et al., 1998) or high hydration (Chiu et al., 1999b), comparable to corresponding x-ray scattering data at low hydration (Weiner and White, 1992a,b) and at high hydration (Tristram-Nagle et al., 1998). Hristova and White (1998) have studied DOPC bilayers at intermediate levels of hydration using x-ray diffraction, in which bromine labeling of the double bonds was used to probe structural changes within the hydrocarbon core. They observed a break point in the hydration-level dependence of the Bragg spacing around 12 waters/lipid, suggesting that the hydration shell of DOPC is composed of about 12 waters.

Another experimental technique that has been used to probe the hydration-level dependence of lipid membranes is nuclear magnetic resonance (NMR). In particular, analysis of deuterium NMR residual quadrupolar splittings of selectively deuterated lipids in multilayered liposomes (Bechinger and Seelig, 1991; Ulrich and Watts, 1994) has provided evidence for lipid headgroup structural changes with the lowering of the bilayer water content below ~13–18

waters/lipid. Spin-lattice relaxation rates of heavy water in multilayered liposomes, in contrast, have indicated that saturation of the lipids with water is essentially complete at ~20–22 waters/lipid (Volke et al., 1994).

Given the data from different experimental techniques, it would be useful to study the hydration of DOPC bilayers at intermediate hydration levels using computer simulations. In particular, simulations in general can complement experimental studies because both the structural and dynamic aspects of these systems may be studied simultaneously.

MODEL AND METHODS

Our general approach for preparing systems at different levels of hydration is to begin with a patch of a fully hydrated DOPC bilayer and incrementally reduce hydration level. From a fully hydrated, equilibrated patch of membrane consisting of 128 DOPC and 4825 water molecules (Chiu et al., 1999b), a thin strip of water molecules near the midplane of the interlamellar region was removed. The resulting opposing water faces were brought close together, and any bad contacts were removed by a brief energy relaxation.

Two cycles, each consisting of 30 ps of molecular dynamics (MD) and 5000 steps of configurational-bias Monte Carlo (CBMC), were performed to help the new systems relax further. This hybrid simulation procedure has been shown to be more effective than pure MD in bringing bilayers to equilibrium (Chiu et al., 1999a). Repetition of the water removal and relaxation steps afforded several unequilibrated systems at the hydration levels of 5.4, 11.4, 16, 23, and 30 waters/lipid (690, 1460, 2048, 2944, and 3840 waters total, respectively). These systems served as potential starting points for independent equilibration using many MD-CBMC cycles, but, for this study, we focused on equilibrating the systems around the Hristova–White break point, i.e., those systems containing 5.4, 11.4, and 16 waters/lipid.

The MD portions of MD-CBMC equilibration cycles were carried out with the area of the membrane, pressure normal to the membrane, and system temperature restrained to specified values using a weak-coupling method (Berendsen et al., 1984). The pressure normal to the bilayer was maintained at 1 atm with 4-ps relaxation time, and the lipids and water were independently coupled to thermal baths at 305 K with a 0.2-ps coupling constant. Values for the membrane area set point (with 4-ps coupling) were obtained from the area per lipid, A_L, estimated from a volumetric relationship (Nagle and Wiener, 1988) among the water volume, the lipid volume, and Bragg spacing: $A_L = 2(V_L + n_W V_W)/D$, where V_L is the volume of a lipid molecule, V_W is the volume of a water molecule, n_W is the number of waters per lipid, and D is the experimental x-ray Bragg spacing at various hydration levels (Hristova and White, 1998). Procedures for extracting volumetric data of lipid components from simulations (Petrache et al., 1997) to aid in interpreting experimental data were previously applied to DOPC (Armen et al., 1998) to obtain a lipid volume of 1302 Å^3 for low hydration. Lipid volumes of 1296 Å^3 at 23°C at low hydration ($n_W = 5.4$) (Wiener and White, 1992a) and 1303.3 Å^3 at 30°C and high hydration ($n_W = 32.5$) (Tristram-Nagle et al., 1998) have also been reported. Given the small dependence of lipid volume on temperature and hydration level, we used $V_L = 1300$ Å^3. We assumed an experimental water volume of 30.0 Å^3 (Lide, 1990), which is close to the simulation-based value of 30.4 (Petrache et al., 1997). The calculated values of A_L, to which our systems were restrained, are listed in Table 1.

Several adjustments to the MD-CBMC cycle protocol (Chiu et al., 1999a) were made to facilitate the lipids and water coming to equilibrium. The number of attempted CBMC moves was doubled from 5,000 to 10,000, and the length of the MD portion was shortened from 30 to 20 ps. Together, these changes tend to favor a larger number of lipid tail reconfiguration events within a given amount of computer time. The possibility of axial rotations and overall translations of lipid molecules during CBMC was excluded, leading to no significant change in the move acceptance, while greatly decreasing the time needed to test a sample configuration. The compute time required by the CBMC portion of this new protocol was about a factor of 20 less than the original protocol (Chiu et al., 1999a) and was ~30–40% of the total compute time for a given MD-CBMC cycle, depending on the level of hydration.

TABLE 1 Area per lipid set points used in the simulations

n_W	A_L (Å^2)
5.4	59.6
11.4	65.2
16	65.8
23	66.7
30	67.6

Interaction parameters for the lipid headgroups, lipid chains, and water were previously described (Chiu et al., 1999b,c, and refs. therein) for incorporation into the GROMOS simulation package (van Gunsteren et al., 1996). A united atom model was used for the lipids, wherein the van der Waals parameters for the hydrocarbon tails were adjusted to fit specific volume data for linear hydrocarbons over a range of chain length and saturation (Chiu et al., 1999c). The SPC/E water model, which reproduces the experimentally observed bulk water density and self-diffusion constant near 305 K (Berendsen et al., 1987), was used. We have verified that SPC/E water closely tracks the temperature dependence of the water self-diffusion coefficient (S.-W. Chiu, unpublished results). Molecular dynamics proceeded by the Verlet leap-frog integration method with a time step of 2 fs. A group-based twin-range cutoff scheme was used for the nonbonded interactions. For groups within 10 Å of each other, the nonbonded interactions were calculated at every time step. Nonbonded interactions were cutoff at 20 Å (Alper et al., 1993a,b; Chiu et al., 1995). The nonbonded pair list for those groups interacting at 10–20 Å were updated every 25 time steps. The boundary conditions were periodic in three dimensions, and the center-of-mass motion was regularly corrected to zero. The SHAKE algorithm (Ryckaert et al., 1977) was used to constrain all bonds lengths to a tolerance of 10^{-4}. The results for the 5.4 waters/lipid system were not significantly affected by turning off the SHAKE algorithm.

Analysis of average distributions and structure

Distributions of molecular fragments were quantified using two different statistical methods. The first method gives the average distance $\langle z \rangle$ from the bilayer center and the standard width σ as simple weighted averages,

$$\langle z \rangle = \sum_i p_i z_i, \quad \sigma^2 = \sum_i p_i (z_i - \langle z \rangle)^2, \tag{1}$$

where p_i is the probability of the fragment being located in the z_i bin. Eqs. 1 were applied to each leaflet separately without symmetrization, and the results were averaged. The second method is a simultaneous fit to a sum of two Gaussian distributions that effectively symmetrizes the distributions,

$$p(z) = \left(\frac{N}{2A\sqrt{\pi}}\right)\left\{\exp\left[-\left(\frac{z - Z}{A}\right)^2\right] + \exp\left[-\left(\frac{z + Z}{A}\right)^2\right]\right\}, \tag{2}$$

where N is the scale factor for each fragment type (Wiener and White, 1992b), Z is the position of the peaks relative to the bilayer center, and A is the $1/e$ half-width. Nonlinear least-squares fitting of Eq. 2 was performed unweighted using the Marquardt method (Marquardt, 1963).

The order parameter S_{CD}, describing the average orientation of the CD bond vector with respect to the bilayer normal (z) direction, is defined as (Seelig, 1977)

$$S_{CD} \equiv S_{zz} = \langle 3\cos^2\theta - 1\rangle/2, \quad (3)$$

where θ is the angle between the CD bond vector and the bilayer normal. Because our systems use implicit nonpolar hydrogens, the bond vectors are reconstructed assuming a tetrahedral geometry. For the choline terminal methyl groups, the first hydrogen atom is reconstructed with a dihedral angle of 180° before rebuilding the remaining hydrogens. The methyl configurations consequently depend on the choline configuration and do not freely rotate.

Chemical shift anisotropy (CSA) as measured by NMR can be used as a measure of the average orientation of a particular molecular group. For lipids in fluid membranes undergoing rotational averaging about a director (taken to be along the z direction), the CSA takes the form (Seelig, 1978)

$$\mathrm{CSA} = S_{11}(\sigma_{11} - \sigma_{22}) + S_{33}(\sigma_{33} - \sigma_{22}), \quad (4)$$

where σ_{ii} are the static principal values of the chemical shielding tensor, and S_{ii} are the order parameters describing the orientation of the appropriate shielding tensor with respect to the bilayer normal. The orientation of the shielding tensor can be measured experimentally from the orientational dependence of the NMR chemical shift. For a first approximation of the phosphate CSA for the simulations, the phosphate shielding tensor was taken as oriented with one axis bisecting the O–P–O angle of nonesterified oxygens, one axis perpendicular to the plane of this angle, and the third axis perpendicular to these two axes (Seelig, 1978). Herzfeld et al. (1978), using single crystals of barium diethyl phosphate as a model for the phospholipid headgroup, have reported that the phosphate shielding tensor is rotated by ~10° from each of these axes. Following the approach of Scherer and Seelig (1989) for POPC lipid bilayers, we approximated the static principal values for the DOPC phosphate group by using the parameters for DPPC (at full hydration and −110°C), with $\sigma_{11} = -81$ ppm, $\sigma_{22} = -21$ ppm, and $\sigma_{33} = 108$ ppm. The hydration-level dependence of the DPPC principal values (Herzfeld et al., 1978) was taken into account by applying linear interpolation to the tabulated values. For calculating carbonyl CSAs, experimental examination of dimethyl oxalate crystals has placed the σ_{22} axis of the carbonyl shielding tensor nearly along the carbonyl bond and the σ_{11} axis in the plane of the sp^2 carbonyl carbon toward the ester linkage, with principal values of $\sigma_{11} = -93$ ppm, $\sigma_{22} = 39$ ppm, and $\sigma_{33} = 54$ ppm (Cornell, 1986). Accordingly, we assumed that σ_{22} is aligned with the carbonyl bond.

Analysis of dynamics

Deuterium relaxation rates as measured by NMR can be used to characterize the dynamics of lipid headgroups and of water. The fluctuating part of the quadrupolar Hamiltonian, responsible for the relaxation process, corresponds to the orientational fluctuations of the CD bond vectors with respect to the external magnetic field. Because the electrostatic field gradients of CD bonds have been found to be approximately axially symmetric (Seelig, 1977), the bond fluctuations are described by the collection of autocorrelation functions,

$$G_m(t) = (4\pi/5)[\langle Y_{2,m}(\Omega; t)Y^*_{2,m}(\Omega; 0)\rangle - |\langle Y_{2,m}(\Omega; t)\rangle|^2], \quad (5)$$

where $Y_{\ell,m}(\Omega; t)$ are time-dependent, second-order spherical harmonic functions (Brown, 1996). The angles Ω represent the coordinate transformation from the principal axis system of the molecule to the laboratory axis system. The spectral densities, which manifest as experimental relaxation rates, are given by the Fourier transforms of the autocorrelation functions,

$$J_m(\omega) = \int_{-\infty}^{\infty} G_m(t)\exp(-i\omega t)\,dt. \quad (6)$$

For deuterium quadrupole relaxation, the spin-lattice relaxation time T_1 is given by (Brown, 1996)

$$\frac{1}{T_1} = \frac{3}{4}\pi^2\chi^2[J_1(\omega_D) + 4J_2(2\omega_D)], \quad (7)$$

where ω_D denotes the nuclear Larmor frequency, and χ is the static quadrupole coupling constant for a given CD bond. Known values for the static quadrupole coupling constant are 222 kHz for heavy water (Volke et al., 1994) and ~170 kHz and ~135 kHz for the choline methylene and N-methyl groups, respectively (Tamm and Seelig, 1983; Seelig, 1977). It is assumed that the static quadrupole coupling constant is independent of lipid hydration level because the quadrupolar interaction is largely intramolecular (Brown, 1996). For isotropically averaged bonds, as may occur for small unilamellar vesicles and generally those molecules whose rotation rates are much faster than the spin-lattice relaxation time, the relaxation rate is given by (Brown, 1979)

$$\frac{1}{T_1} = \frac{3}{8}(2\pi\chi)^2(1 - S_{CD}^2)\tau. \quad (8)$$

In general, only small differences exist between the T_1 times of unsonicated bilayers and small vesicles (Brown, 1996).

The bond autocorrelation functions $G_m(t)$ from the three 500-ps intervals at each simulated hydration level were averaged. The slow decay of these functions was approximated using a three-parameter fit involving a single effective exponential time constant τ,

$$f(t) = f_\infty + (f_0 - f_\infty)\exp(-t/\tau). \quad (9)$$

The resulting spectral densities from Eq. 6 take the analytic form,

$$J(\omega \neq 0) = 2(f_0 - f_\infty)\tau/(1 + \tau^2\omega^2). \quad (10)$$

RESULTS AND DISCUSSION

The systems at hydration levels of 5.4, 11.4, and 16 waters/lipid were subject to multiple MD-CBMC simulation cycles until equilibrium was judged to have been attained as evidenced by plateaus in the total system potential energy, simulated Bragg spacing, and area per lipid, shown in Figs. 1 and 2. Simulation at each hydration level concludes with three 600-ps MD intervals, each separated by a CBMC sequence. Figure 3 shows the membrane surface tension over time. In these simulations the surface tension is an emergent property because it is not imposed by the simulation. Because the instantaneous surface tension is a rapidly varying quantity, for ease of viewing, the data has been smoothed using a 100-ps moving window average. The observed positive surface tensions on the order of a few tens of dyn/cm are of the same order of magnitude as the surface tension inferred from monolayer experiments (Chiu et al., 1995). Below, we further analyze the last 500 ps of each interval, giving a total of 1.5 ns of data for each of these hydration levels. In addition, a single 500-ps trajectory from an earlier equilibrated DOPC simulation at

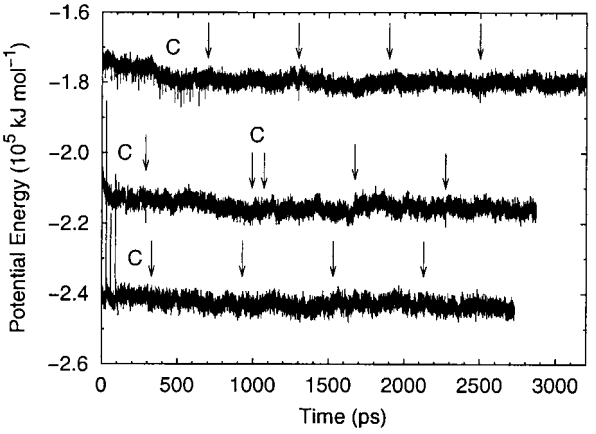

FIGURE 1 Total system potential energy vs. time for hydration levels of 5.4 (*top*), 11.4 (*middle*) and 16 (*bottom*) waters/lipid. The labels *C* between arrows indicate regions where MD-CBMC cycles were used, and the arrows indicate where CBMC intervened between long, continuous molecular dynamics trajectories.

high hydration (37.7 waters/lipid)(Chiu et al., 1999b) was analyzed for spin-lattice relaxation times and headgroup order parameters.

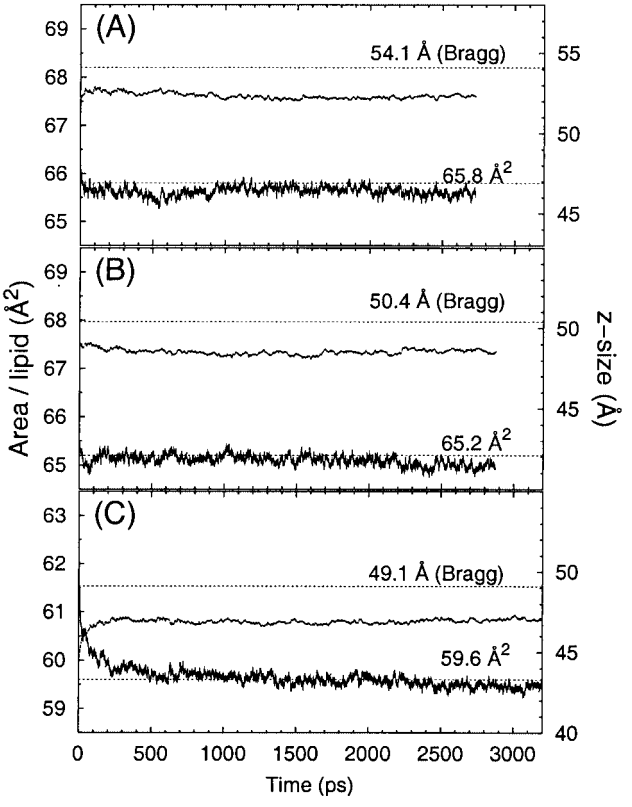

FIGURE 2 Area per lipid and *z*-dimension of the simulation unit cell versus time for hydration levels of (*A*) 16, (*B*) 11.4, and (*C*) 5.4. The dashed lines correspond to the experimental values of the Bragg spacing (based on Table 1 of Hristova and White; 1998 and the area-per-lipid set point derived from volumetric considerations (see Table 1) used in the simulations.

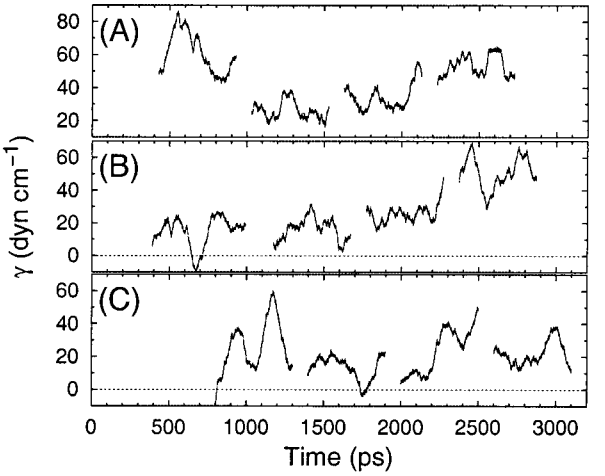

FIGURE 3 Membrane surface tension versus time for hydration levels of (*A*) 16, (*B*) 11.4, and (*C*) 5.4 waters/lipid, smoothed using a 100-ps moving average.

Bilayer structure

Figure 4 shows the simulated transbilayer neutron and x-ray scattering profiles at several hydration levels, with comparison to results from the joint refinement of x-ray and neutron scattering data for 5.4 waters/lipid (Wiener and White, 1992b). The low-hydration simulation reproduces the peak positions of both types of scattering experiments well, but gives a larger electron density in the bilayer interior. There also appears to be little variation within the hydrocarbon core for 5.4 to 16 waters/lipid.

Figure 5 shows the internal structure of the simulated bilayer at low hydration, with comparison to the density distributions of the various molecular fragments from joint refinement (Wiener and White, 1992b). The peak positions of the simulated distributions are in reasonable agreement with experiment. Figure 5 *A* shows particularly good agreement for the double-bond distribution and the positions of the carbonyl, water, and methyl distributions. Qualitative differences include slightly broader simulated widths for the carbonyl, water, and methyl distributions and a water distribution that extends more deeply into the bilayer. The overall chain methylene distribution is slightly narrower than that from experiment and has a substantially higher number density near the bilayer center. This is likely why the simulated Bragg spacing is about 5% less than the experimental value of 49.1 Å (Wiener and White, 1992b; Hristova and White, 1998). In Fig. 5 *B*, the simulated carbonyl and glycerol distributions appear slightly broader and the phosphate distribution appears slightly narrower when compared to the experimental joint refinement distributions. The simulated phosphate and choline distributions appear to be comparably distributed.

The simulated molecular fragment distributions at low hydration are quantified in Table 2. For a given molecular

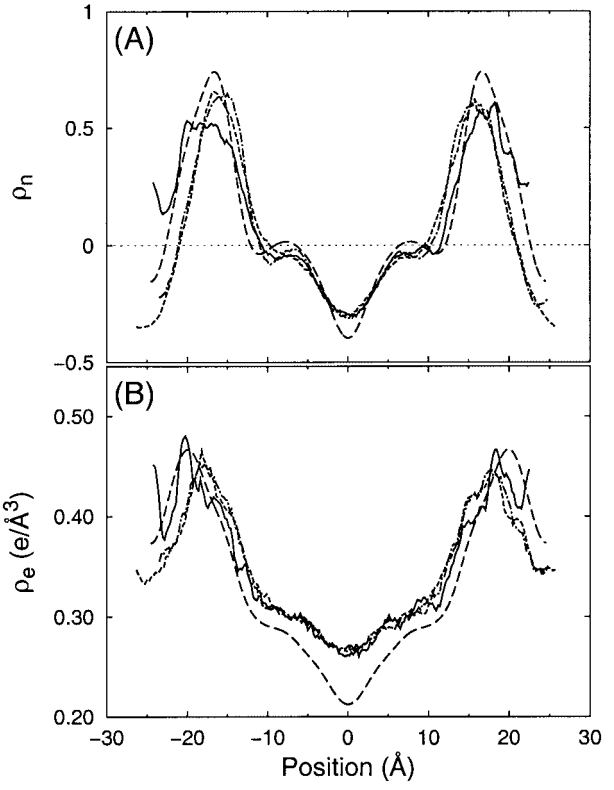

FIGURE 4 Simulated unsymmetrized transbilayer (*A*) neutron and (*B*) x-ray scattering density profiles at hydration levels of 16 (*short dashed*), 11.4 (*dot dashed*), and 5.4 (*solid*) waters/lipid. Results from joint refinement of x-ray and neutron scattering studies at 5.4 waters/lipid (CALC2 parameters in Table 3 of Wiener and White, 1992b) is shown for comparison (*long dashed*). The profiles are positioned relative to the center of the bilayer, and the units of density are (*A*) scattering length per unit length $\times 10^4$ and (*B*) e/Å^3.

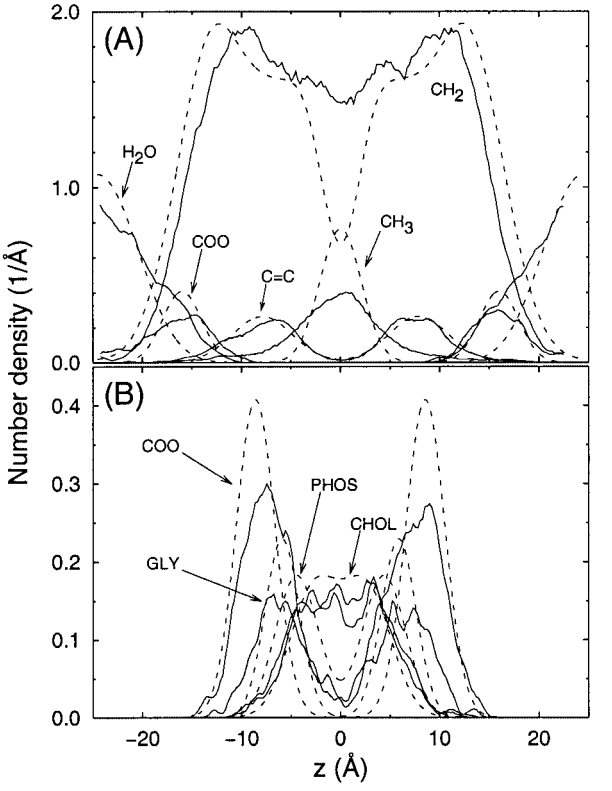

FIGURE 5 Simulated unsymmetrized distributions of molecular fragments (*solid*), relative to the average midplanes of (*A*) the bilayer and (*B*) the interlamellar space, for 5.4 waters/lipid. Experimental distributions (*dashed*) are the result of joint refinement of x-ray and neutron diffraction data (see Fig. 4). The experimental and simulated Bragg spacings were 49.1 Å and 46.9 Å, respectively.

fragment, the average peak positions resulting from the different averaging methods are in agreement. The half-widths computed in the present work (columns II and III) are slightly broader than those obtained from joint refinement (Wiener and White, 1992b) or those obtained in previous all-atom DOPC simulations (Feller et al., 1997). Results from the weighted average analysis (Eq. 1) for the systems with hydration levels of 11.4 and 16 waters/lipid are given in Table 3. For these hydration levels, there is a very low amount of interpenetration of phosphocholine groups from apposing bilayers, unlike at low hydration.

Figure 6, *A–C*, show a comparison between the simulated Bragg spacings, carbonyl distances, and double-bond distributions with those obtained using x-ray diffraction (Hristova and White, 1998; Wiener et al., 1991). The simulated molecular fragments distributions appearing in Fig. 6, *B–C*, are based on analysis using the symmetrizing dual-Gaussian function (Eq. 2). Analysis of the fragment distributions for 5.4 waters/lipid (see Table 2, column II) using the weighted average method, in contrast, shows that the simulated carbonyl distance and double bond position are brought into closer agreement with experiment. The fraction of hydrocarbon thickness of the bilayer, D_{HC}, shown in Fig. 6 *D* does not suggest a strong trend with hydration. Small differences in the simulated double-bond position and half-widths, as compared to experiment, appear to contribute to this difference. We find in Fig. 6, *A–C*, that the raw simulation data values differ from experiment on the order of only a few percent, giving good agreement overall.

Lipid order parameters and chemical shift anisotropies

Order parameters can be used to provide information about lipid chain and headgroup configurations. Figure 7 *A* shows the hydrocarbon chain order parameters. Because the simulated order parameters for the *sn*-1 and *sn*-2 chains were found to be very similar to each other for a given hydration level, the order parameters shown here are averaged over both chains. In addition to the characteristic dip at carbon 10 due to the double bond, there is a systematic ordering in the chains upon dehydrating the bilayer. In the 5.4 waters/lipid system, the chain order parameters for carbons 3–7 are in

TABLE 2 Values of average positions (as measured from the bilayer center) and widths of molecular fragment distributions for the 5.4 waters/lipid hydration level

	Position, $\langle z \rangle$ or Z (Å)				Width, σ (Å)			
	I*	II*	III†	IV‡	I	II	III	IV
Choline	21.86	20.52	20.38 ± 0.03	21.89 ± 0.13	2.14	3.09	2.67 ± 0.05	2.46 ± 0.39
Phosphate	21.18	19.90	19.93 ± 0.04	20.19 ± 0.08	1.85	2.58	2.72 ± 0.05	2.18 ± 0.06
Glycerol	18.28	17.22	17.16 ± 0.04	18.67 ± 0.38	1.85	2.69	2.79 ± 0.03	1.68 ± 0.22
Carbonyl	16.62	16.05	15.90 ± 0.04	15.97 ± 0.02	1.92	2.80	2.86 ± 0.03	1.93 ± 0.04
C═C	8.66	7.96	7.56 ± 0.05	7.88 ± 0.09	2.82	3.33	3.20 ± 0.04	3.03 ± 0.11
Methyl	−0.14	0.00	0.00 ± 0.05	0.0	4.38	4.87	4.17 ± 0.04	2.09 ± 0.20

*Methods I (all-atom DOPC lipids, Feller et al., 1997) and II (this work) use a weighted average and sample deviation (Eqs. 1).
†Method III (this work) uses a curve fit to a sum of two Gaussian distributions (Eq. 2) with $\sigma = A/\sqrt{2}$.
‡From joint refinement of x-ray and neutron diffraction data (Wiener and White, 1992b).

good agreement with previously published all-atom DOPC simulations at this hydration level (Feller et al., 1997), and those for carbons 11–17 were found to be systematically more disordered than theirs by about 0.05.

By convention, the methylene segments of the choline group are labeled α and β, and the methyl segments are labeled γ, i.e., $–PO_4–C^{(\alpha)}H_2–C^{(\beta)}H_2–N(C^{(\gamma)}H_3)_3$. The simulated choline order parameters shown in Fig. 7 *B* reveal that increasing the hydration level does not appear to produce a substantial effect on the headgroup order. Alternatively, the average orientation of the P–N vectors in each of the leaflets was evaluated directly. We found that, on average, the headgroups were inclined 10.7°, 10.6°, 9.7°, and 8.0° from parallel to the bilayer surface for the hydration levels of 37.7, 16, 11.4, and 5.4 waters/lipid, respectively. (The average standard deviations trended from ~23° to 27° in going from high to low hydration.) Thus, the headgroups became more parallel to the membrane by about 3° as the water content was lowered. This result supports experimental ^{2}H-NMR studies of deuterated headgroups of DOPC (Ulrich and Watts, 1994) and of POPC (Bechinger and Seelig, 1991). In those studies, it was shown that the quadrupolar frequency splittings of the choline segments trended with hydration level, approaching plateau values ~13–18 waters/lipid. That trend was interpreted by those authors as evidence for a conformational change of the headgroups.

TABLE 3 Values of average positions and widths of molecular fragment distributions for the 11.4 and 16 waters/lipid hydration levels*

	Position, $\langle z \rangle$ (Å)		Width, σ (Å)	
n_w =	11.4	16	11.4	16
Choline	19.42	19.35	2.84	3.12
Phosphate	18.68	18.53	2.45	2.58
Glycerol	15.97	15.85	2.31	2.50
Carbonyl	14.85	14.72	2.28	2.54
C═C	7.08	7.06	2.85	3.14
Methyl	2.02	1.99	4.72	4.72

*Obtained from weighted averages and sample deviations (Eqs. 1).

Chemical shift anisotropy

The phosphate CSA measures the average orientation of the phosphate group. Using the shielding tensor orientation described by Seelig (1978), simulated CSAs of −29, −21, and −15 ppm for 5.4, 11.4, and 16 waters/lipid, respectively, were obtained. Accounting for the shielding tensor reorientation (Herzfeld et al., 1978) modifies all computed CSAs by ~−3 ppm, and accounting for the hydration-level effects on the principal values of the shielding tensor (Herzfeld et al., 1978) modifies our computed CSAs by ~+3 ppm. Experimental ^{31}P-NMR measurements of DOPC bilayers have yielded phosphate CSAs of −36 ppm (at presumably full hydration)(Sanders et al., 1991) and ~−50 ppm (at 30°C and various hydration levels) (Ulrich and Watts, 1994). Given the variation among the experimentally reported CSAs themselves, we find that the simulated values are in reasonable agreement with experiment.

Likewise, carbonyl CSAs from our simulations were −19, −9, and −16 ppm for the hydration levels of 5.4, 11.4, and 16 waters/lipid, respectively. Experimental ^{13}C-NMR studies by Smith et al. (1992) have afforded *sn*-1 carbonyl CSAs for pure DPPC bilayers (−32 ppm at 46°C), for DPPC in egg PC bilayers (−28 ppm at 24–28°C), and, for dipalmitoylglycerol in egg PC bilayers (−24 ppm at 24–28°C). If the variation in experimental carbonyl CSAs were found to vary to the extent that was found in the literature for phosphate CSAs, then our results compare well with NMR experiments, suggesting that the simulated average *sn*-1 carbonyl orientation is similar to that indicated by experiment.

Choline spin-lattice relaxation rates

Spin-lattice relaxation rates as a function of hydration have been computed from the simulations to study the general motion of the choline group. For the asymptotic fit (Eq. 9) to the orientational autocorrelation function (Eq. 5), the simulations generally yielded the effective time constants τ in the range 70–200 ps, with f_0 of order 0.1 and f_∞ of order 0.01. The simulated $1/T_1$ relaxation rates for the cholines

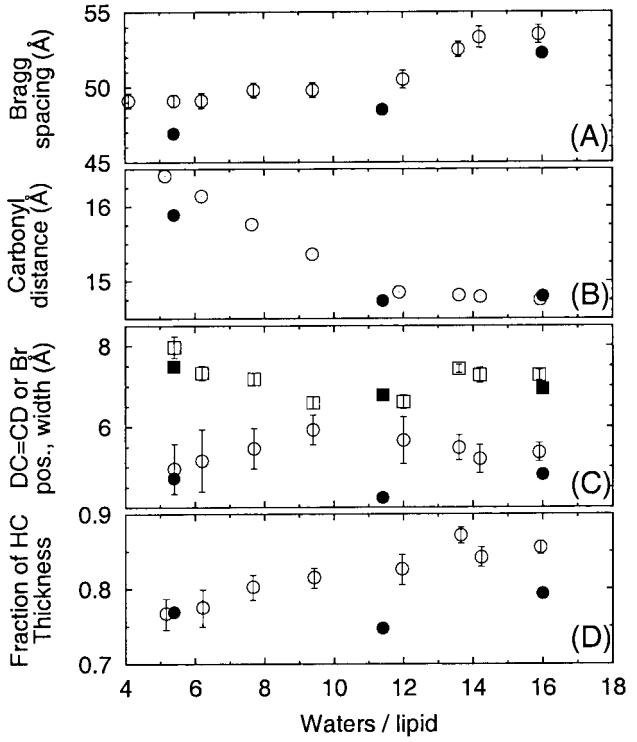

FIGURE 6 Bilayer structure as a function of hydration level, for simulated data (*filled symbols*) and for experimentally derived data (*open symbols*). (*A*) Bragg spacings (from Table 1 of Hristova and White, 1998). (*B*) Average carbonyl distance, D_{HC}, as measured from the bilayer center. Simulated values were obtained from a dual-Gaussian fit (see Eq. 2) to the COO molecular fragment distribution. Experimental values (Fig. 9 of Hristova and White, 1998) were based on volumetric predictions using x-ray Bragg spacings. (*C*) Peak positions (*squares*, Z_{Br}), as measured from the bilayer center, and 1/*e* half-widths (*circles*, A_{Br}) describing the distribution of the double bonds. Simulated data was obtained from a dual-Gaussian fit to the $^2HC{=}C^2H$ fragment using reconstructed ^2H atom positions (bond length, 1.0 Å). Experimental values (Table 1 of Hristova and White, 1998; Wiener et al., 1991) were obtained from x-ray diffraction of isomorphous DOPC specifically brominated at the *sn*-2 double bond. (*D*) Fraction of hydrocarbon (HC) thickness, equal to the ratio $(Z_{Br} + A_{Br})/D_{HC}$.

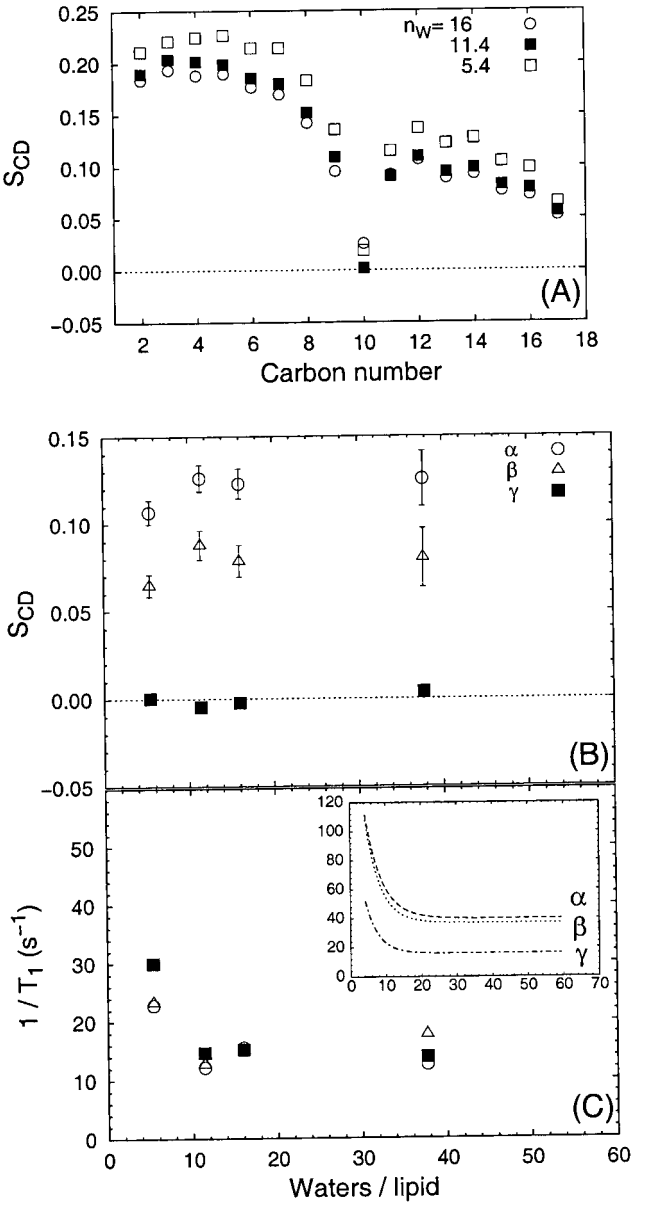

FIGURE 7 (*A*) Simulated order parameters of reconstructed CD bonds for the hydrocarbon tails (averaged over both chains). (*B*) Simulated choline order parameters. Error bars = 1σ. (*C*) Simulated spin-lattice relaxation rates for the choline segments, based on Eq. 7. (*C*, *inset*) The curve fittings to experimental choline ^2H-NMR relaxation data at 30°C for multilamellar liposomes (Ulrich and Watts, 1994).

were computed using the full relaxation expression given by Eq. 7. Figure 7 *C* shows that all three choline segments undergo a dynamic response to hydration, with evidence of a break point at ~11 waters/lipid. This plateauing of the relaxation rates is in rough agreement with the rates observed in ^2H-NMR experiments for multilamellar liposomes (Ulrich and Watts, 1994) (see Fig. 10 *C*, *inset*), with experimental plateau values of 16–40 s^{-1} at high hydrations in comparison to the ~14–20 s^{-1} suggested by our simulations. A more precise comparison is not possible because our simulations are too short to sample these relatively slow motions accurately.

Water dynamics and organization

NMR studies have indicated that water molecules associated with the lipid headgroups are in exchange with bulk water (Lazrak et al., 1987; Pope and Cornell, 1979). To test whether this exchange could reasonably occur on the MD time scale studied here, the mean-square displacement for those waters remaining in the headgroup hydration shell during the last 20 ps of each of the nine data sets (three for each hydration level) was computed. We find a value of ~0.05 $Å^2$/ps, corresponding to a headgroup water moving, on average, about 5.2 Å, or several water diameters, during the 600 ps from which a data set is produced. Tables 2 and

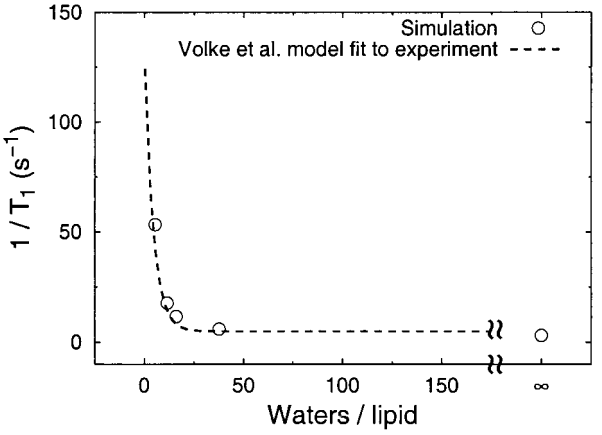

FIGURE 8 Spin-lattice relaxation rates of H_2O as a function of hydration level as calculated from simulation using Eq. 8. Infinite hydration corresponds to the result from a separate calculation using bulk SPC/E water. The broken line is a fit to experimental relaxation times of ^2H_2O in multilamellar DOPC bilayers (Volke et al., 1994).

3 indicate that the peak-to-peak distance between the simulated carbonyl and choline distributions is approximately 5 Å. The amount of simulation time is therefore reasonably sufficient to allow for the exchange of headgroup waters.

Experimental ^{2}H-NMR studies measuring effective deuterium quadrupole splittings $\Delta\nu_Q$ of heavy water in DOPC bilayer dispersions as a function of hydration have been performed by Volke et al. (1994), who found that the effective splitting decreases monotonically with increasing hydration level. Using the relation $\Delta\nu_Q = \frac{3}{4}\chi S_{CD}$ from their work, one obtains from their curve fit the equivalent S_{CD} values of 0.011, 0.0060, 0.0044, and 0.0019, with estimated standard error 0.001, for hydration levels of 5.4, 11.4, 16, and 37.7 waters/lipid, respectively. The values obtained directly from our simulations using H_2O were, respectively, -0.031, -0.014, -0.011, and -0.004, with standard error 0.01. The corresponding simulated $\langle\cos^2\theta\rangle$ values evaluated using Eq. 3 were systematically lower but within 10% of the corresponding experimental values, making for good agreement.

Spin-lattice relaxation rates for heavy water have also been measured with ^{2}H-NMR by Volke et al. (1994), who found that it is a rapidly decreasing function of lipid hydration level. Figure 8 compares the simulated $1/T_1$ rates for water, evaluated using Eq. 8 and the simulated S_{CD} water order parameters listed above, to the curve fit to their experimental data. Even though the simulated range of hydration levels is much smaller than was studied experimentally (up to 200 waters/lipid), the simulations indicate the formation of a plateau ~20–25 waters/lipid. This agreement with experimental findings suggests that the water reorientational dynamics in the experimental and simulated systems are similar.

Another measure of water dynamics is given by the effective lateral self-diffusion coefficient. Using pulsed field gradient ^{1}H-NMR, Volke et al. (1994) have measured the effective H_2O self-diffusion coefficient in nonoriented POPC bilayers, showing a sigmoidal dependence on hydration level. Based on our simulations, the slope of the water mean-square displacement curve from 4 to 10 ps afforded average water lateral diffusion coefficients of $(2.8 \pm 0.5) \times 10^{-10}$, $(9.1 \pm 1.0) \times 10^{-10}$, and $(14.6 \pm 1.0) \times 10^{-10}$ m^2/s, for 5.4, 11.4, and 16 waters/lipid, respectively. This trend indicates that water mobility is restricted by the membrane surface. These values are approximately twice those reported experimentally. To understand this difference, we note that the asymptotic bulk water lateral diffusion coefficient as reported for the Volke et al. model is 10.9×10^{-10} m^2/s, which is about half the experimentally established value of 22.6×10^{-10} m^2/s (Gray, 1972). The simulated average lateral water diffusion coefficients, normalized to bulk diffusion, however, agree closely with the experimental NMR data.

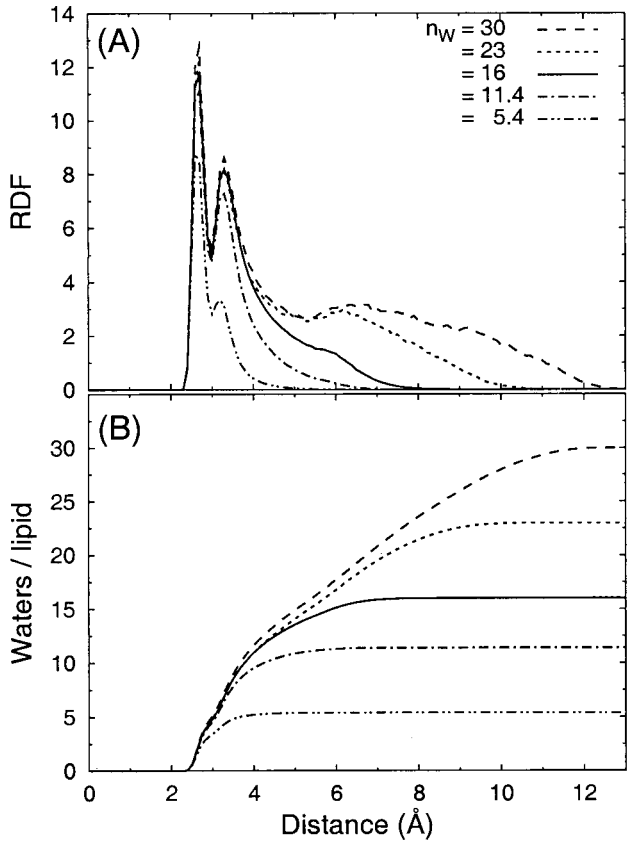

FIGURE 9 (*A*) Radial distribution functions for waters to the nearest DOPC headgroup atoms, for several hydration levels from simulation. (*B*) The cumulative areas under the RDF curves.

One a level of detail that simulations can provide is the distribution of water molecules around the headgroup. Figure 9 *A* is a variation of the traditional radial distribution function (RDF), showing the distances between the water oxygens and only the nearest headgroup atoms. The two

distinct peaks appearing at all hydration levels are located at ~2.6–2.7 Å and ~3.2–3.3 Å. Decomposition of both peaks into atom groups revealed that the phosphorus oxygens, and, to a lesser extent, the carbonyls, comprise the inner peak, and the choline terminal methyls and methylenes and the glycerol carbons, in decreasing order of importance, give rise to the outer peak. The RDF at 5.4 waters/lipid observed for simulations of all-atom DOPC bilayers (i.e., with explicit hydrogen atoms), in contrast, seem to have only one peak (S. Feller, personal communication). The existence of two peaks may therefore be due to slight variations in the effective sizes of the united headgroup atoms. The hydration dependence is as follows. As the hydration level is reduced from high hydration down to 16 waters/lipid, the magnitudes of both peaks remain constant. In going from 16 to 11.4 waters/lipid, the height of the outer peak begins to fall first, indicating that the inner peak corresponds to the more tightly bound waters. Finally, in going from 11.4 to 5.4 waters/lipid, the heights of both the inner and outer peaks decrease.

The average number of waters in the hydration shell can be estimated by integrating the RDFs, normalizing to give the numbers of waters per lipid, and reading off the value at a distance of about one water molecule beyond the climbing phase of the curve. In Fig. 9 *B*, the climbing phase for each system ends near 3.0 Å. The numbers of waters in the hydration shell, found in the range 4.0–4.5 Å, is estimated to be ~11–13 for $n_W = 16$ and greater. Our earlier work on fully hydrated DOPC membranes at $n_W = 37.7$ (Chiu et al., 1999b) is in good agreement. For $n_W = 11.4$, we estimate 9–10 waters in the hydration shell, and, for $n_W = 5.4$, virtually each water molecule is in some hydration shell. These results support the hypothesis that ~12 waters/lipid marks the completion of the DOPC hydration shell (Hristova and White, 1998).

Finally, dipole potentials for the variously hydrated DOPC systems were computed, and the peak values occuring in the aqueous layer are plotted in Fig. 10. For all hydration levels studied, the water contributed a negative potential, and the lipids contributed a positive potential, relative to the interlamellar region. For hydration levels of $n_W = 16$ and greater, the total dipole potential was ~−500 mV, and, after dehydration of the bilayer, it increased to ~−300 mV for $n_W = 11.4$ and to ~+400 mV for $n_W = 5.4$. To understand the origin of this sign reversal, we decomposed the total dipole potential into various contributions, also shown in Fig. 10. It is seen that, in going from 11.4 to 5.4 waters/lipid, there is a switch in the relative magnitudes of the dipole potential due to the phosphocholine and due to the total dipole potential phosphocholine. From this result, it is inferred that the sign reversal of the total dipole potential is in part due to the dehydration of the phosphocholine group. This reversal may be connected with the closer proximity of phosphocholine groups from apposing bilayers in going from the 11.4 to 5.4 waters/lipid hydration level, as revealed in the molecular fragment distributions in Fig. 5 *B*. Because experimental measurements of the dipole potential are performed at full hydration or in excess water (Gawrisch et al., 1992; Clarke, 1997), there is, to our knowledge, no direct experimental evidence of a sign reversal of the dipole potential upon dehydration of the membrane.

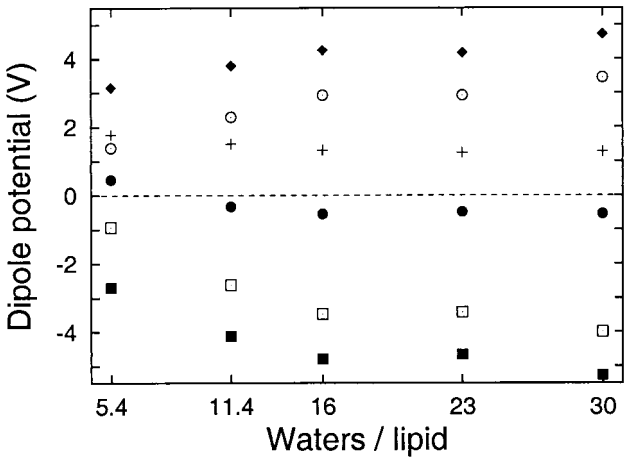

FIGURE 10 Peak values of the simulated total dipole potential (●) near the center of the aqueous interlamellar region as a function of hydration level. Various contributions to the total dipole potential are shown: water (■); entire lipid (▲); phosphocholine (○); glycerol and lipid tails (+); and water, glycerol, and lipid tails (i.e., total dipole minus phosphocholine) (□).

CONCLUSION

We have performed molecular dynamics simulations of DOPC bilayers at different hydration levels to investigate headgroup hydration and the structure and dynamics of both the lipid and water components. Areas in which the simulations showed agreement with experiment include the following: x-ray and neutron scattering profiles at low hydration, the peak positions of the molecular fragment distributions at low hydration, peak positions of the carbonyl and double-bond distributions as a function of hydration, average order parameters and spin-lattice relaxation rates for water molecules as a function of hydration, lipid orientations as measured by chemical shift anisotropy, and variation of water mobility as a function of hydration. Furthermore, a plateau effect in spin-lattice relaxation rates of the headgroup in response to hydration, similar to that seen in NMR experiments, was obtained, but it is likely that simulations of several nanoseconds' duration would be necessary to quantify these rates accurately. Although the widths of the P–N vector distributions and the choline segment relaxation response to hydration indicate that the headgroup is capable of undergoing a substantial range of motion, we observed an increased alignment of the average

lipid headgroup with the bilayer surface in lowering the water content. In addition, the surface dipole potential showed a reversal in sign in going from 11.4 to 5.4 waters/lipid due to the depletion of the headgroup hydration shell. Other analyses support the notion that the DOPC headgroup can accommodate ~12 waters/lipid in its hydration layer. Given the wide range of observable quantities with which to compare, we find that our simulations generally appear to be in good agreement with experimental results.

Computer time for this work was provided by the National Center for Supercomputing Applications and used the SGI Origin 2000. Financial support from the National Science Foundation and from the National Institutes of Health is gratefully acknowledged.

REFERENCES

Alper, H. E., D. Bassolino, and T. R. Stouch. 1993a. Computer simulations of a phospholipid monolayer-water system: the influence of long range forces on water structure and dynamics. *J. Chem. Phys.* 98:9798–9807.

Alper, H. E., D. Bassolino-Klimas, and T. R. Stouch. 1993b. The limiting behavior of water hydrating a phospholipid monolayer: a computer simulation study. *J. Chem. Phys.* 99:5547–5559.

Armen, R. S., O. D. Uitto, and S. E. Feller. 1998. Phopholipid component volumes: determination and application to bilayer structure calculations. *Biophys. J.* 75:734–744.

Bechinger, B., and J. Seelig. 1991. Conformational changes of the phosphatidylcholine headgroup due to membrane dehydration. A ^{2}H-NMR study. *Chem. Phys. Lipids.* 58:1–5.

Berendsen, H. J. C., J. R. Grigera, and T. P. Straatsma. 1987. The missing term in effective pair potentials. *J. Phys. Chem.* 91:6269–6271.

Berendsen, H. J. C., J. P. M. Postma, W. F. van Gunsteren, A. DiNola, and J. R. Haak. 1984. Molecular dynamics with coupling to an external bath. *J. Chem. Phys.* 81:3684–3690.

Berger, O., O. Edholm, and F. Jahnig. 1997. Molecular dynamics simulations of a fluid bilayer of dipalmitoylphosphatidylcholine at full hydration, constant pressure, and constant temperature. *Biophys. J.* 72: 2002–2013.

Bloom, M., E. Evans, and O. Mouritsen. 1991. Physical properties of the fluid lipid bilayer component of cell membranes: a perspective. *Q. Rev. Biophys.* 24:293–397.

Brown, M. F. 1979. Deuterium relaxation and molecular dynamics in lipid bilayers. *J. Magn. Res.* 35:203–215.

Brown, M. F. 1996. Membrane structure and dynamics studied with NMR spectroscopy. *In* Biological Membranes. K. M. Merz and B. Roux, editors. Birkhäuser, Boston, MA.175–252.

Brown, M. F., A. A. Ribeiro, and G. D. Williams. 1983. New view of lipid bilayer dynamics from ^{2}H and ^{13}C NMR relaxation time measurements. *Proc. Nat. Acad. Sci. U.S.A.* 80:4325–4329.

Brown, M. F., J. Seelig, and U. Häberlen. 1979. Structural dynamics in phospholipid bilayers from deuterium spin-lattice relaxation time measurements. *J. Chem. Phys.* 70:5045–5053.

Chiu, S.-W., M. Clark, S. Subramaniam, H. L. Scott, and E. Jakobsson. 1995. Incorporation of surface tension in to molecular dynamics simulations of an interface: a fluid phase lipid bilayer membrane. *Biophys. J.* 69:1230–1245.

Chiu, S.-W., M. M. Clark, E. Jakobsson, S. Subramaniam, and H. L. Scott. 1999a. Application of a combined Monte Carlo and molecular dynamics method to the simulation of a diplamitoyl phosphatidylcholine lipid bilayer. *J. Comput. Chem.* 20:1153–1164.

Chiu, S.-W., E. Jakobsson, S. Subramaniam, and H. L. Scott. 1999b. Combined Monte Carlo and molecular dynamics simulation of fully hydrated dioleoyl and palmityoyl-oleyl phosphatidylcholine lipid bilayers. *Biophys. J.* 77:2462–2469.

Chiu, S.-W., M. M. Clark, E. Jakobsson, S. Subramaniam, and H. L. Scott. 1999c. Optimization of hydrocarbon chain interaction parameters: application to the simulation of fluid phase lipid bilayers. *J. Phys. Chem. B.* 103:6323–6327.

Clarke, R. J. 1997. Effect of lipid structure on the dipole potential of phosphatidylcholine bilayers. *Biochem. Biophys. Acta.* 1327:269–278.

Cornell, B. A. 1986. Chemical shielding tensors of C-13 in solid dimethyl oxalate. *J. Chem. Phys.* 85:4199–4201.

Damodaran, K. V., and K. M. Merz. 1994. A comparison of DMPC and DLPE-based lipid bilayers. *Langmuir.* 9:1179–1183.

Egberts, E., S. J. Marrink, and H. J. C. Berendsen. 1994. Molecular dynamics simulation of a phospholipid membrane. *Eur. Biophys. J.* 222:423–436.

Feller, S. E., Y. Daxu, R. W. Pastor, and A. D. MacKerell, Jr. 1997. Molecular dynamics simulation of unsaturated lipid bilayers at low hydration: parameterization and comparison with diffraction studies. *Biophys. J.* 73:2269–2279.

Feller, S. E., D. Huster, and K. Gawrisch. 1999. Interpretation of NOESY cross-relaxation rates from molecular dynamics simulation of a lipid bilayer. *J. Am. Chem. Soc.* 121:8963–8964.

Feller, S. E., Y. Zhang, and R. W. Pastor. 1994. Computer simulation of liquid/liquid interfaces II. Surface tension-area dependence of a bilayer and monolayer. *J. Chem. Phys.* 103:10267–10276.

Gawrisch, K., D. Ruston, J. Zimmerbery, V. A. Parsegian, R. P. Rand, and N. Fuller. 1992. Membrane dipole potentials, hydration forces, and the ordering of water at membrane surfaces. *Biophys. J.* 61:1213–1223.

Gray, D. E., editor. 1972. American Institute of Physics Handbook. McGraw-Hill, New York.

Herzfeld, J., R. G. Griffin, and R. A. Haberkorn. 1978. P-31 chemical-shift tensors in barium diethyl phosphate and urea-phosphoric acid: model compounds for phospholipid headgroup studies. *Biochemistry.* 17: 2711–2718.

Hristova, K., and S. H. White. 1998. Determination of the hydrocarbon core structure of fluid DOPC bilayers by x-ray diffraction using specific bromination of the double-bonds: effect of hydration. *Biophys. J.* 74: 2419–2433.

Huang, P., J. J. Perez, and G. H. Loew. 1994. Molecular dynamics simulations of phospholipid bilayers. *J. Biomol. Struct. Dyn.* 11: 927–956.

Husslein, T., D. M. Newns, P. C. Pattnaik, Q. Zhong, P. B. Moore, and M. Klein. 1998. Constant pressure and temperature molecular dynamics simulation of the hydrated diphytanolphosphatidylcholine lipid bilayer. *J. Chem. Phys.* 109:2826–2832.

Jakobsson, E. 1997. Computer simulation studies of biological membranes: progress, promise, and pitfalls. *Trends Biochem. Sci.* 9:339–354.

Lazrak, T., A. Milon, G. Wolff, A. M. Albrecht, M. Miele, G. Ourisson, and Y. Nakatani. 1987. Comparison of the effects of inserted C_{40}- and C_{50}-terminally dihydroxylated carotenoids on the mechanical properties of various phospholipid vesicles. *Biochim. Biophys. Acta.* 903:132–141. See also Erratum. 1988. *Biochim. Biophys. Acta.* 22:427.

Lide, D. R., editor. 1990–1991. CRC Handbook of Chemistry and Physics. CRC Press, Boca Raton, FL.

Lindahl, E., and O. Edholm. 2000. Mesoscopic undulations and thickness fluctuations in lipid bilayers from molecular dynamics simulations. *Biophys. J.* 79:426–433.

Marquardt, D. W. 1963. An algorithm for least-squares estimation of non-linear parameters. *J. Soc. Indust. Appl. Math.* 11:431–441.

McIntosh, T. J. 1990. X-ray diffraction analysis of membrane lipids. *In* Molecular Description of Biological Membrane Components by Computer Aided Conformational Analysis. Brasseur, R., editor. CRC Press, Boca Raton, FL.

Mendelsohn, R., and L. Senak. 1993. Quantitative determination of conformational disorder in biological membranes by FTIR spectroscopt. *In* Biomolecular Spectroscopy. J. R. Clark, and R. E. Heister, editors. Wiley, New York.

Merz, K., and B. Roux, editors. 1996. Biological Membranes: A Molecular Perspective from Computation and Experiment. Birkhauser, Boston, MA.

Nagle, J. F., and M. C. Wiener. 1988. Structure of fully hydrated bilayer dispersions. *Biochim. Biophys. Acta.* 942:1–10.

Pastor, R. 1994. Molecular dynamics and Monte Carlo simulations of lipid bilayers. *Curr. Opin. Struct. Biol.* 4:443–464.

Petrache, H. I., S. E. Feller, and J. F. Nagle. 1997. Determination of component volumes of lipid bilayers from simulations. *Biophys. J.* 72: 2237–2242.

Pope, J. M., and B. A. Cornell. 1979. A pulsed NMR study of lipids, bound water and sodium ions in macroscopically oriented lecithin/water lyotropic liquid crystal model membrane systems. *Chem. Phys. Lipids.* 24:27–43.

Ryckaert, W. E., G. Ciccotti, and H. J. C. Berendsen. 1977. Numerical integration of the Cartesian equations of motion of a system with constraints: molecular dynamics of *n*-alkanes. *J. Comput. Phys.* 23: 327–341.

Sanders, J. C., T. W. Poile, R. B. Spruijt, N. A. J. Van Nuland, A. Watts, and M. A. Hemminga. 1991. A NMR investigation of the interactions of the α-oligomeric form of the M13 coat protein with lipids, which mimic the *E. coli* inner membrane. *Biochem. Biophys. Acta.* 1066:102–108.

Scherer, P. G., and J. Seelig. 1989. Electric charge effects on phospholipid headgroups. Phosphatidylcholine in mixtures with cationic and anionic amphiphiles. *Biochemistry.* 28:7720–7728.

Seelig, J. 1977. Deuterium magnetic resonance: theory and application to lipid membranes. *Q. Rev. Biophys.* 10:353–418.

Seelig, J. 1978. ^{31}P NMR and the headgroup structure of phospholipids in membranes. *Biochim. Biophys. Acta.* 515:105–140.

Smith, S. O., I. Kustanovich, S. Bhamidipati, A. Salmon, and J. A. Hamilton. 1992. Interfacial conformation of dipalmitoylglycerol and dipalmitoylphosphatidylcholine in phospholipid bilayers. *Biochemistry.* 31:11660–11664.

Stouch, T. 1993. Lipid membrane structure and dynamics studied by all-atom molecular dynamics simulations of hydrated phospholipid bilayers. *Mol. Sim.* 10:317–335.

Tamm, L. K., and J. Seelig. 1983. Lipid solvation of cytochrome *c* oxidase. Deuterium, N-14, and P-31 NMR studies on the phosophocholine headgroup and on *cis*-unsaturated fatty acyl chains. *Biochemistry.* 22: 1474–1483.

Tieleman, D. P., and H. J. C. Berendsen. 1996. Molecular dynamics simulations of a fully hydrated dipalmitoylphosphatidylcholine bilayer with different macroscopic boundary conditions and parameters. *J. Chem. Phys.* 105:4871–4880.

Tieleman, D. P., S. J. Marrink, and H. J. C. Berendsen. 1997. A computer perspective of membranes: molecular dynamics of lipid bilayer systems. *Biochim. Biophys. Acta.* 1331:235–270.

Tristram-Nagle, S., R. Zhang, R. M. Suter, C. R. Worthington, W. J. Sun, and J. F. Nagle. 1993. Measurement of chain tilt angle in fully hydrated bilayers of gel phase lecithins. *Biophys. J.* 64:1097–1109.

Tristram-Nagle, S., H. I. Petrache, and J. F. Nagle. 1998. Structure and interactions of fully hydrated DOPC bilayers. *Biophys. J.* 75:917–925.

Tu, K., D. Tobias, and M. Klein. 1995. Constant pressure and temperature molecular dynamics simulation of a fully hydrated liquid crystal phase dipalmitoylphosphatidylcholine. *Biophys. J.* 69:2558–2562.

Ulrich, A. S., and A. Watts. 1994. Molecular response of the lipid headgroup to bilayer hydration monitored by ^{2}H-NMR. *Biophys. J.* 66: 1441–1449.

van Gunsteren, W. F., S. R. Billeter, A. A. Eising, P. H. Hünenberger, P. Krüger, A. E. Mark, W. R. P. Scott, and I. G. Tironi. 1996. Biomolecular simulation: the Gromos96 manual and user guide. Vdf Hochschulverlag AG an der ETH Zürich, Zürich, Switzerland. (or see http://igc.ethz.ch/gromos/).

Venable, R., B. Zhang, B. Hardy, and R. Pastor. 1993. Molecular dynamics simulations of a lipid bilayer and of hexadecane: an investigation of membrane fluidity. *Science.* 262:223–226.

Volke, F., S. Eisenblätter, J. Galle, and G. Klose. 1994. Dynamic properties of water at phosphatidylcholine lipid-bilayer surfaces as seen by deuterium and pulse field gradient proton NMR. *Chem. Phys. Lipids* 70: 121–131.

Wiener, M. C., G. I. King, and S. H. White. 1991. Structure of a fluid DOPC bilayer determined by joint refinement of x-ray and neutron diffraction data. *Biophys. J.* 60:568–576.

Wiener, M. C., and S. H. White. 1992a. Structure of a fluid dioleoylphosphatidylcholine bilayer determined by joint refinement of x-ray and neutron diffraction data II. Distribution and packing of terminal methyl groups. *Biophys. J.* 61:428–433.

Wiener, M. C., and S. H. White. 1992b. Structure of a fluid dioleoylphosphatidylcholine bilayer determined by joint refinement of x-ray and neutron diffraction data III. Complete structure. *Biophys. J.* 61: 434–447.

Wong, P. T. T., and H. H. Mantsch. 1988. Reorientational and conformation ordering processes at elevated pressures in 1,2-dioleoyl phosphatidylcholine. *Biophys. J.* 54:781–790.

Zhou, Z., B. G. Sayer, D. W. Hughes, R. E. Stark, and R. M. Epand. 1999. Studies of phospholipid hydration by high-resolution magic-angle spinning nuclear magnetic resonance. *Biophys. J.* 76:387–399.